REPORT DOCUMENTATION PAGE

Form Approved
OMB No. 0704-0188

PLEASE DO NOT RETURN YOUR FORM TO THE ABOVE ADDRESS.

1. REPORT DATE *(DD-MM-YYYY)*	2. REPORT TYPE	3. DATES COVERED *(From - To)*
20-03-2011	Journal Paper	01-10-2008 - 30-09-2009

4. TITLE AND SUBTITLE

Effects of Surface Treatment and Interfacial Strength on the Damage Propagation in Layered Transparent Armor Under Impact
---Effects of Loading Rates and Surface Conditions on Flexural Strength of Borosilicate Glass

5a. CONTRACT NUMBER

54666EG

5b. GRANT NUMBER

W911NF0810533

5c. PROGRAM ELEMENT NUMBER

6. AUTHOR(S)

Weinong Wayne Chen

5d. PROJECT NUMBER

5e. TASK NUMBER

5f. WORK UNIT NUMBER

7. PERFORMING ORGANIZATION NAME(S) AND ADDRESS(ES)

Purdue University
Sponsored Programs Services
West Lafayette, IN 47907-2108

8. PERFORMING ORGANIZATION REPORT NUMBER

9. SPONSORING/MONITORING AGENCY NAME(S) AND ADDRESS(ES)

Dr. Ralph Anthenien
U.S. Army Research Office
P.O. Box 12211
Research Triangle Park, NC 27709-2211

10. SPONSOR/MONITOR'S ACRONYM(S)

ARO

11. SPONSOR/MONITOR'S REPORT NUMBER(S)

54666EG

12. DISTRIBUTION/AVAILABILITY STATEMENT

Approved for public release; federal purpose rights.

13. SUPPLEMENTARY NOTES

14. ABSTRACT

This study evaluates the loading-rate and surface-condition dependence of flexural strength of a borosilicate glass. The tensile surfaces of glass bending specimens are subjected to 3 different surface treatments. Four-point bending experiments are performed on those treated samples, at loading rates ranging from 0.7 MPa/s to 4×10^6 MPa/s. The results show that the flexural strength of the borosilicate glass increases with increasing loading rate. When the surface is chemically etched, the flexural strength increases by an order of magnitude and fracture initiates from an edge. The high strength measured in the etched glass is still far less than the intrinsic tensile strength, indicating a flaw-determined failure.

15. SUBJECT TERMS

16. SECURITY CLASSIFICATION OF:			17. LIMITATION OF ABSTRACT	18. NUMBER OF PAGES	19a. NAME OF RESPONSIBLE PERSON
a. REPORT	b. ABSTRACT	c. THIS PAGE			19b. TELEPHONE NUMBER *(Include area code)*

Reset

INSTRUCTIONS FOR COMPLETING SF 298

1. REPORT DATE. Full publication date, including day, month, if available. Must cite at least the year and be Year 2000 compliant, e.g. 30-06-1998; xx-06-1998; xx-xx-1998.

2. REPORT TYPE. State the type of report, such as final, technical, interim, memorandum, master's thesis, progress, quarterly, research, special, group study, etc.

3. DATES COVERED. Indicate the time during which the work was performed and the report was written, e.g., Jun 1997 - Jun 1998; 1-10 Jun 1996; May - Nov 1998; Nov 1998.

4. TITLE. Enter title and subtitle with volume number and part number, if applicable. On classified documents, enter the title classification in parentheses.

5a. CONTRACT NUMBER. Enter all contract numbers as they appear in the report, e.g. F33615-86-C-5169.

5b. GRANT NUMBER. Enter all grant numbers as they appear in the report, e.g. AFOSR-82-1234.

5c. PROGRAM ELEMENT NUMBER. Enter all program element numbers as they appear in the report, e.g. 61101A.

5d. PROJECT NUMBER. Enter all project numbers as they appear in the report, e.g. 1F665702D1257; ILIR.

5e. TASK NUMBER. Enter all task numbers as they appear in the report, e.g. 05; RF0330201; T4112.

5f. WORK UNIT NUMBER. Enter all work unit numbers as they appear in the report, e.g. 001; AFAPL30480105.

6. AUTHOR(S). Enter name(s) of person(s) responsible for writing the report, performing the research, or credited with the content of the report. The form of entry is the last name, first name, middle initial, and additional qualifiers separated by commas, e.g. Smith, Richard, J, Jr.

7. PERFORMING ORGANIZATION NAME(S) AND ADDRESS(ES). Self-explanatory.

8. PERFORMING ORGANIZATION REPORT NUMBER. Enter all unique alphanumeric report numbers assigned by the performing organization, e.g. BRL-1234; AFWL-TR-85-4017-Vol-21-PT-2.

9. SPONSORING/MONITORING AGENCY NAME(S) AND ADDRESS(ES). Enter the name and address of the organization(s) financially responsible for and monitoring the work.

10. SPONSOR/MONITOR'S ACRONYM(S). Enter, if available, e.g. BRL, ARDEC, NADC.

11. SPONSOR/MONITOR'S REPORT NUMBER(S). Enter report number as assigned by the sponsoring/ monitoring agency, if available, e.g. BRL-TR-829; -215.

12. DISTRIBUTION/AVAILABILITY STATEMENT. Use agency-mandated availability statements to indicate the public availability or distribution limitations of the report. If additional limitations/ restrictions or special markings are indicated, follow agency authorization procedures, e.g. RD/FRD, PROPIN, ITAR, etc. Include copyright information.

13. SUPPLEMENTARY NOTES. Enter information not included elsewhere such as: prepared in cooperation with; translation of; report supersedes; old edition number, etc.

14. ABSTRACT. A brief (approximately 200 words) factual summary of the most significant information.

15. SUBJECT TERMS. Key words or phrases identifying major concepts in the report.

16. SECURITY CLASSIFICATION. Enter security classification in accordance with security classification regulations, e.g. U, C, S, etc. If this form contains classified information, stamp classification level on the top and bottom of this page.

17. LIMITATION OF ABSTRACT. This block must be completed to assign a distribution limitation to the abstract. Enter UU (Unclassified Unlimited) or SAR (Same as Report). An entry in this block is necessary if the abstract is to be limited.

journal

J. Am. Ceram. Soc., 92 [6] 1287–1295 (2009)
DOI: 10.1111/j.1551-2916.2009.03019.x

Effect of Loading Rate and Surface Conditions on the Flexural Strength of Borosilicate Glass

Xu Nie and Weinong W. Chen†

AAE and MSE Schools, Purdue University, West Lafayette, Indiana 47907-2045

Andrew A. Wereszczak

Oak Ridge National Laboratory, Oak Ridge, Tennessee 37831-6068

Douglas W. Templeton

US Army Tank and Automotive Research and Development, Warren, Michigan 48397-5000

This study evaluates the loading rate and surface condition dependence of the flexural strength of a borosilicate glass. The glass specimens are subjected to three different surface treatments before four-point bending tests to study the effect of surface flaws. Quasistatic (Material Test System 810) and dynamic (Kolsky bar) experiments are performed at loading rates ranging from 0.7 to 4×10^6 MPa/s. The results show that the flexural strength of the borosilicate glass has a strong dependence on the loading rate. A chemically etched surface produces an enhanced flexural strength by about an order of magnitude. Scanning electron microscopy images on fracture surfaces indicate that the failure is governed by different types of flaws under different surface treatment conditions. Edge failure is also identified for samples possessing high flexural strength.

I. Introduction

Recent research on the dynamic compressive response of borosilicate glass showed that the glass is capable of bearing up to 1.5 GPa uniaxial compression stress before cracks propagate extensively in the specimen.[1] The dynamic deformation and fracture behavior of this glass under multiaxial compression was studied with the specimen confined by steel collars in a Kolsky bar or split Hopkinson pressure bar (SHPB).[2] However, it has been shown that under ballistic impact loading conditions, the most dominant and vital failure modes are spalling and bending-induced tension on the back side of the glass plate,[3] which points to the need for determining the dynamic tensile failure behavior under high-rate bending. Under flexural loading, glass strength is typically limited by surface defects introduced by after-manufacturing handling, but rarely by bulk defects.[4] Therefore, for the glasses in blast-resisting window applications, it is important to understand the loading rate and surface condition effects on the tensile or the flexural strength.

Under quasistatic loading conditions, intensive research efforts have been made toward exploring the influence of various surface treatments on the flexural strengths of glass and ceramic materials during the past decades.[5–11] It has been identified that surface conditions play a significant role in the fracture strength and crack propagation of glasses.[8–11] Compared with ceramics, glass materials are more susceptible to surface flaws due to the lack of bulk defects.[4] Although the theoretical strength of glass is considered to be in the order of 10 GPa at room temperature,[12] very little work has been reported on the achievement of this strength under laboratory conditions mostly due to the improper handling of glass samples and the moisture effect in the testing environment.

Different methods to improve the surface quality of oxide glasses have been reviewed in Donald.[13] As a conclusion, surface etching is considered to be one of the most effective and simple methods to remove or reduce surface defects. The principle for surface etching is to either remove surface cracks completely or blunt the crack tip significantly through material removal. Bulk glass strengths exceeding 1 GPa have been produced by this method.[14,15] Recent research results on the ballistic response of thin glass plates have revealed a significantly enhanced impact resistance in an HF acid-etched glass target.[3] No fracture was initiated on the back side of the glass plate target, which was in tension, at impact speeds of up to 700 m/s. In this study, although the effects of surface modification on impact resistance are clearly shown, the surface morphologies of treated and untreated glass and their influences on the material strength were not documented. It is of significant interest to establish the relationship between dynamic flexural strength and surface conditions in order to optimize the ballistic resistance in light transparent armors.

In this paper, we studied the loading rate and surface condition effects on the flexural strength of a borosilicate glass utilizing a Kolsky bar with its testing section modified into a four-point bending configuration. The tensile surfaces of the bending specimens are modified into three different surface conditions as follows: ground by 220-grit sandpapers, ground by a 1500-grit sandpaper, and polished and etched by 5 wt% HF acid. Grinding directions are perpendicular to the surface tensile stress direction. The morphology of the treated surfaces is characterized by scanning electron microscopy (SEM) and atomic force microscopy (AFM). Detailed surface features and roughness values are given in this paper. A high-speed camera is synchronized with the SHPB to capture the crack initiation and propagation in the glass specimens. It was found that the flexural strength decreases with increasing surface roughness for ground samples, while the etched samples possess the highest strength although at high surface roughness. This indicates that the surface roughness may not be the critical parameter that determines the tensile strength of glass materials. When the loading rate increases, the strength increases for all the surface conditions. The detailed experimental setup, procedures, and experimental results are presented in the following sections.

V. Sglavo—contributing editor

Manuscript No. 24917. Received June 29, 2008; approved February 5, 2009.
This work was partially supported by the U.S. Army Research Office under Grant No. W911-05-1-0218 to Purdue University. Wereszczak was supported by WFO sponsor US Army Tank-Automotive Research, Development, and Engineering Center under contract DE-AC05-00OR22725 with UT-Battelle, LLC.
†Author to whom correspondence should be addressed. e-mail: wchen@purdue.edu

II. Experimental Procedure

(1) Materials and Specimens

The borosilicate glass used in this research was provided by U.S. Army Research Laboratory, Aberdeen Proving Ground, MD, in the form of flat plates. The dimensions and properties of the as-received material were described in a previous paper studying the shear effects on the compressive strength of the same glass.[1] The glass plates were first machined into 2 mm × 3 mm × 30 mm glass prisms, and then polished to a surface finish of 80/50 scratch/dig. All the four edges of the as-received samples were chamfered before surface treatments were performed. The chamfer angle was 45°, with a dimension of approximately 0.12 mm. The polished and chamfered samples were then divided into three groups. The first group was ground with a 220-grit sandpaper, and the second group was ground with a 1500-grit sandpaper. Both grindings were performed only on the tensile surface and were perpendicular to the tensile axis, as shown in Fig. 1. These two groups were denoted as group #1 and group #2, respectively. The specimens from the third group were immersed in 5% HF acid for 15 min. The principle of HF acid etching is that HF in the aqueous solution attacks SiO_2 in the glass to form water-soluble reaction products. In this way, the glass material is stripped off from the surface layer by layer so that the preexisting surface flaws are eliminated. The etching process removed 100–150 μm of glass material from the tensile surface. This group was denoted as group #3. To minimize the interaction between the etched glass and the moisture in the room air, the etched specimens were subjected to mechanical loading within a few minutes after etching.

(2) Strength Testing Methodology

In this study, uniaxial flexural strength experiments are performed instead of uniaxial tensile strength testing, which is very difficult to conduct accurately on brittle materials. The measured flexural strength values are used to make inferences on the uniaxial tensile strength of glass. Four-point bending flexural tests were conducted to evaluate the tensile strengths of the three groups of borosilicate glass samples. A set of four-point bending fixtures were designed according to ASTM C1161-02c. The spacing between the two loading pins and that between two support pins are 10 and 20 mm, respectively. Pin rollers were made of hardened M-2 steel with a hardness of RC 60. These rollers were fixed to the aluminum back fixture. The temperature of the testing environment was 26°C, and the relative humidity was 34%. The low-rate (0.7, 50, and 2500 MPa/s) experiments were performed on a close loop-controlled servohydraulic testing machine (Material Test System [MTS] 810, MTS Corp., Eden, Prairie, MN), while the high-rate experiments were carried out on a modified SHPB setup. SHPB is a well-established apparatus commonly utilized in the high-strain-rate characterization of materials to provide a complete family of dynamic stress–strain curves as a function of strain rates.[16] This technique was initially designed by Kolsky[17] for the characterization of the dynamic flow behavior of ductile materials at strain rates up to 10^4 s^{-1}. The modified versions of this device have been widely used in characterizing the dynamic properties of different materials, such as brittle materials[1,18] and soft materials,[19,20] during the past years. A recent modification of SHPB[21] extends the range of characterization to the dynamic fracture toughness of brittle materials in the four-point bending configuration. This experimental method was designed based on the ASTM Standard C 1421-01b,[22] which specifies the standardized procedure of determining the fracture toughness of ceramics at quasistatic loading rates. To load the specimen at high constant rates while maintaining equilibrated loading across the gauge section, the pulse-shaping technique was used to generate controlled loading profiles. In this research, we adopted the four-point bending fixture design following ASTM Standard C1161-02c[23] for determination of the flexural strength of advanced ceramic materials, and extended the method to high rates.

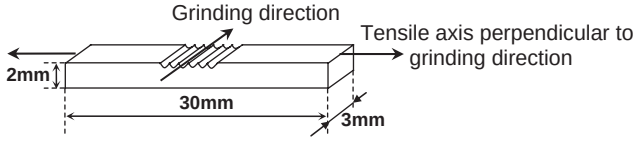

Fig. 1. Surface grinding of bending samples.

In a typical SHPB experiment on brittle materials such as glasses and ceramics, a nearly linear loading pulse is necessary in order to deform the specimen at a nearly constant strain rate.[24–26] This is usually achieved by placing a thin annealed copper disk, called a pulse shaper, between the striker and the incident bar. Ramp loading with different slopes may be generated by adjusting the thickness and diameter of this pulse shaper, as well as the striking velocity. In this research, the specimen is a small glass beam that has a very low stiffness along the loading axis. According to the Eulerian elastic beam theory, a constant loading rate is ensured only when the deflection rate is constant. When the specimen stiffness is very low, the deflection rate is nearly determined by the particle velocity of the loading end of the incident bar, which is in turn determined by the amplitude of the incident pulse. Thus, to achieve a constant deflection rate in the beam specimen, a constant amplitude of the incident pulse is necessary.

Besides the low stiffness, the beam specimens also possess low resonance frequencies that are easily excited by sudden acceleration or deceleration of the loading grips.[27] Although it is inevitable that the specimens have to be accelerated to desired testing conditions and then decelerated back, the process of velocity changes can be controlled to minimize inertia effects. For example, if a step incident pulse is used to achieve the necessary constant amplitude of the incident pulse, the sharp rise in the stress–time profile will excite resonance in the beam specimen. This induces mixing of inertia forces with the mechanical stress in the measured axial load signals, making the resultant data very difficult to explain. The inertia forces also destroy the force equilibrium between the loading and the supporting points on the specimen, making the data reduction uncertain and inaccurate. The high-frequency oscillations that ride on a conventional SHPB incident pulse can also cause inertia problems, in addition to nonconstant loading rates. In this research, in order to generate an incident pulse with both a gradual initial increase and a constant plateau over most of the loading duration without high-frequency oscillations, a thin copper disk of 0.2 mm thickness and 3 mm diameter was placed between the striker and the incident bar as the pulse shaper. Variations in the pulse-shaper dimensions and striking velocity can alter the initial loading rate. The maximum achievable loading rate without sacrificing the force equilibrium across the sample was found to be 4×10^6 MPa/s. Also, in both the servo-hydraulic and the SHPB experiments, a thin Teflon foil was placed between the sample and the roller surfaces to minimize friction and contact-induced stress concentration. The use of a Teflon foil may exert an effect on wave propagation. However, due to the small thickness of the foil, the duration of effect is very short, which is absorbed in the dynamic equilibrium process of the loading.

(3) Glass Surface Characterization and Fractography

Surface roughness value has long been considered as an important parameter describing the surface qualities and therefore, for brittle materials, a critical parameter that can affect the flexural strength.[28,29] Two measures of surface quality that are commonly used are the arithmetic mean roughness value (R_a) and the maximum peak-to-valley height (R_t). The former provides a general picture of surface flaws, while the latter points out the most severe flaw on the surface and is perhaps more relevant to the strength response in a brittle material. In this research, we utilize both SEM and AFM for surface characterization. SEM images provide a surface view over a relatively large area,

and AFM quantifies the selected surface with 3D images and roughness values. It should be noted that the roughness values obtained by a profilometer measurement may vary from those obtained by AFM due to the differences in the areas covered by the two instruments. AFM images provide a more detailed surface flaw distribution than the zigzag curves from profilometers. The limited scan area of AFM image may result in surface roughness values that are not representative of the entire surface. However, the trends of surface roughness variation measured among different surface conditions are consistent by both methods.[8] In the research reported in this article, AFM was used for surface morphology measurements and comparisons. The maximum scanning capability of the AFM we used is 0.1 mm $\times$ 0.1 mm, which is a relatively small area compared with the entire glass surface investigated. For each examined sample, a minimum of 10 AFM images were taken from different parts of the surface to avoid localized results. Surface roughness values (R_a and R_t) of these images were then collected by a computer program and the calculated average values were considered to be the surface property of the sample. Optical microscopy was also used to analyze the fractography of fracture surfaces using the methods outlined in ASTM C1322. In particular, we identified the location of failure initiation under different loading rates and surface conditions. Fracture surfaces from broken samples under six different combinations of testing conditions (two loading rates and three surface treatments) were examined.

III. Experimental Results and Discussions

(1) Glass Surface Features

A typical set of SEM and AFM images for all the three groups of glass samples are displayed in Fig. 2. The corresponding surface roughness values are summarized in Table I. For the purpose of comparison, a set of as-polished surface images are also shown in Fig. 3. It is evident that the polished surfaces show an extremely smooth and flat feature with very few identifiable surface flaws at the magnification of $\times$1800 for the SEM image.

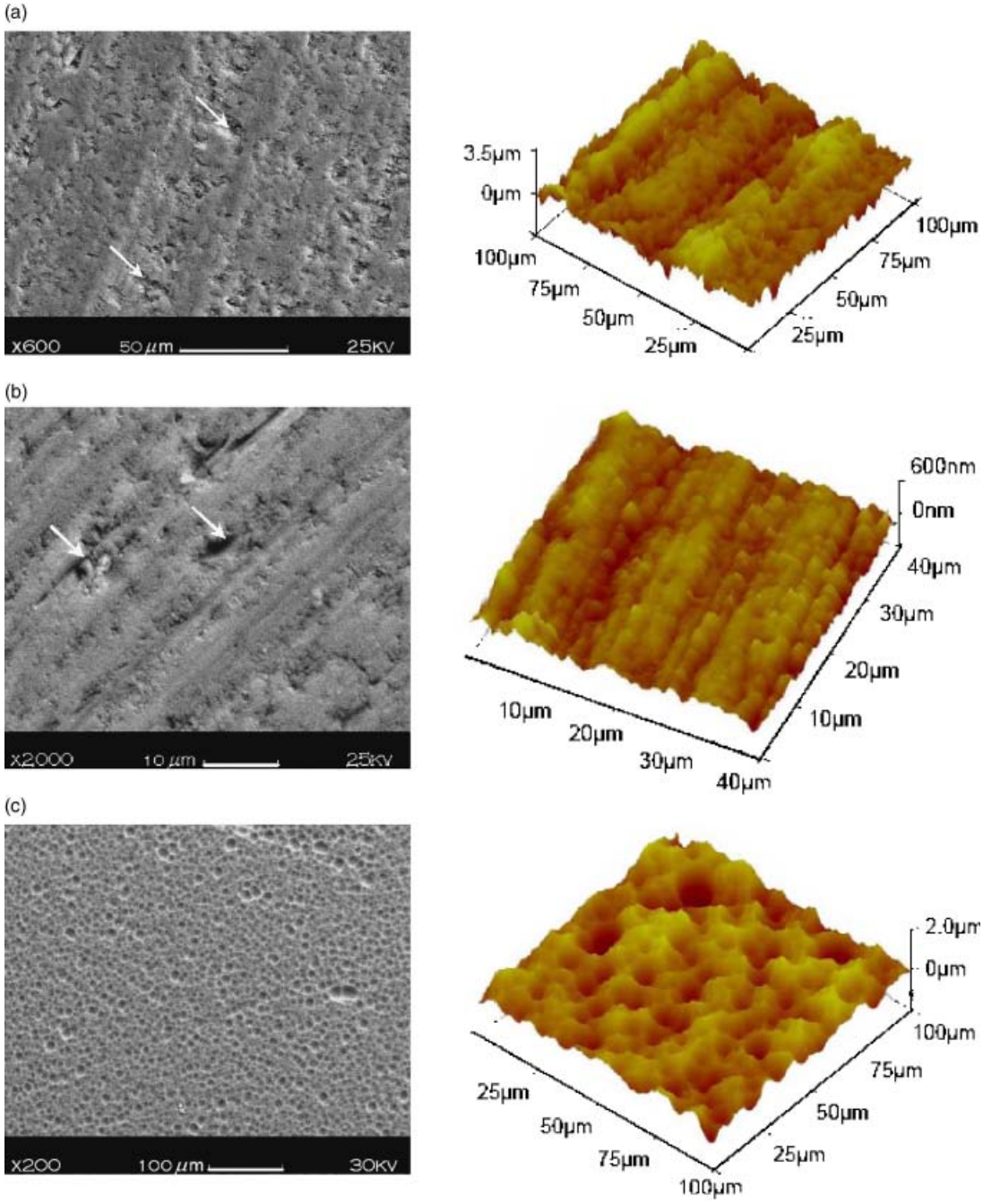

Fig. 2. Glass sample surface morphology of (a) ground by 220-grit sandpaper; (b) ground by 1500-grit sandpaper; (c) polished and etched by HF acid.

Table I. Surface Roughness Values for Different Groups of Samples

	Sample group #1	Sample group #2	Sample group #3
R_a (μm)	0.414	0.0585	0.236
R_t (μm)	3.8	0.725	2.25

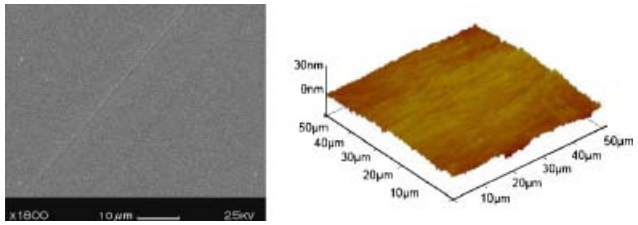

Fig. 3. Glass surface morphology of as-polished samples.

This nearly flaw-free surface provides an ideal base for further surface modifications. Both SEM and AFM images from Fig. 2 revealed two types of major flaws on sample surfaces from groups #1 and #2. Grooves are evident along the grinding direction, suggesting severe deformation caused by particle abrasion. However, the real fracture-initiating flaws are thought to be sharp indentation pits indicated by the white arrows in Figs. 2(a) and (b). These flaws are created by particle indentation on the initially polished surfaces during the grinding process, followed by the formation of new cracks underneath due to the alkali ion-assisted surface reaction between moisture and the silica network.[30] While the glass sample is loaded in four-point bending, stress concentrations around the crack tips increase the local stresses to much higher levels and drive the crack to propagate through the specimen. This failure mode is activated even though the overall stress level in the sample is still very low. The SEM images of Figs. 2(a) and (b) demonstrate a clear comparison in the size differences in those indentation pits created by different grit size sandpaper particles. The relatively small flaw size in Fig. 2(b) indicates a less damaged surface and thus potentially a higher tensile strength. It can be seen that the surface roughness values (both R_a and R_t) for group #2 samples are lower than those of group #1 samples. Figure 2(c) shows a surface morphology after 15 min of HF acid etching on the tensile surfaces of polished samples. It can be seen that the polishing traces are almost completely removed by HF acid etching, leaving rounded pits as the dominant surface features.

A simplified model that describes the surface etching effect on the flexure strength of glass materials is schematically shown in Fig. 4.[31] Similar approaches were used in a more recent study on the bending strength of etched soda-lime glass rods.[32] According to this model, an idealized surface crack is uniformly attacked by acid at every point so that this crack eventually develops into a semicircle. Based on the model, the final radii of these pits are determined by the depth of original cracks. Hence, the observed variation in the pits radii may be directly related to the variation in the initial crack size. Sharp surface flaws are considered to exist widely in glass materials due to mechanical machining, grinding, and polishing, as well as after-manufacturing handling. In our study, the as-received glass surfaces were polished and were flat and smooth as shown in Fig. 3. After etching,

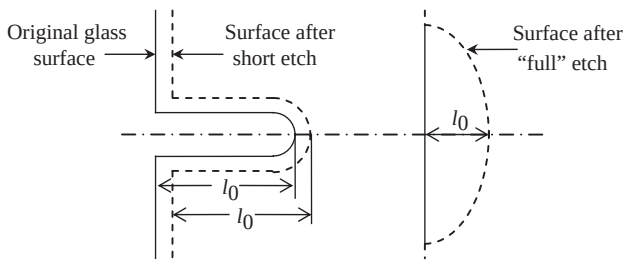

Fig. 4. HF acid etching of an idealized surface flaw.

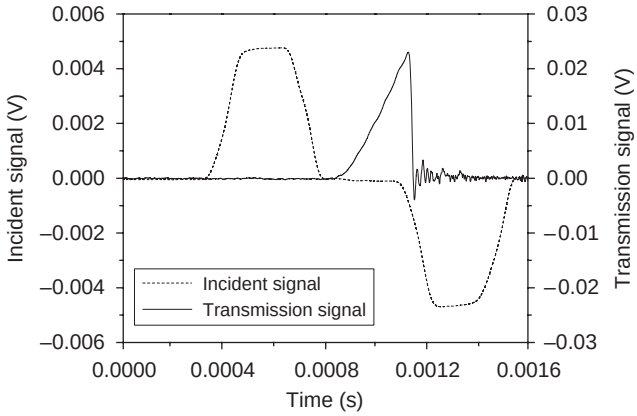

Fig. 5. Original oscilloscope records of a split Hopkinson pressure bar dynamic bending experiment.

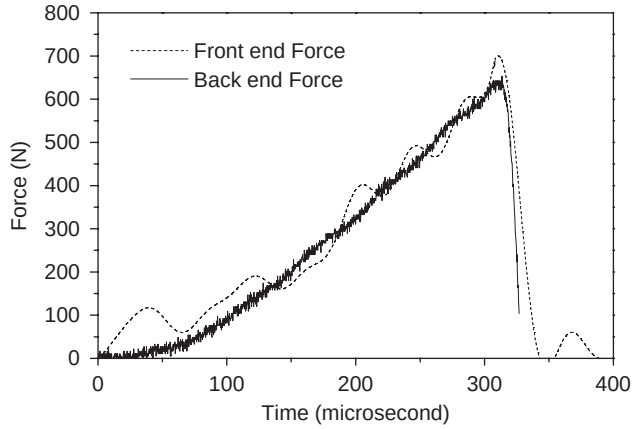

Fig. 6. Force equilibrium histories between the front and back end spans.

the surface morphology transformed into a bumpy pattern as shown in Fig. 2(c). It is believed that a simultaneous acid attack on a series of surface flaws eventually yielded this observed surface pattern. For a sharp, strength-dominating surface crack, the crack tip radius can be in the range of nanometers. After etching, the average radius increases to around 20 μm. The flaw tip rounding achieved by acid attack significantly relieves the stress concentrations at the crack tip when the surface is subjected to tension.

(2) Four-Point Bending Experiments

Four-point bending experiments on glass samples subjected to different tensile surface treatments were conducted at four

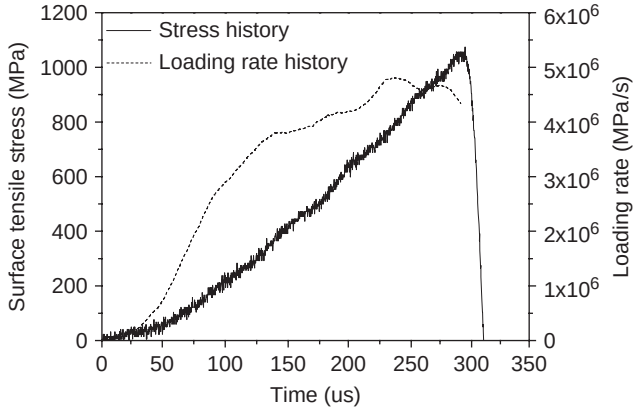

Fig. 7. Loading rate history in a split Hopkinson pressure bar experiment.

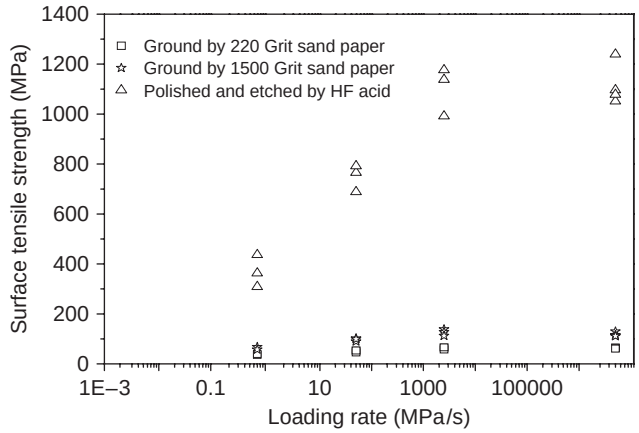

Fig. 8. Loading-rate effects on flexural strength of borosilicate glass with different surface conditions.

different loading rates to investigate the rate effects on flexural strength. Three of the loading rates (0.7, 50, and 2500 MPa/s) were achieved by a servohydraulic testing machine, while a modified SHPB was used to perform experiments at the highest loading rate—4×10^6 MPa/s. A typical set of original oscilloscope recordings of the incident, reflected, and transmitted signals from an SHPB experiment are shown in Fig. 5. It should be noted that the transmitted signal was collected by a pair of semiconductor strain gauges, whose sensitivity is approximately 70 times higher than that of the resistor strain gauges on the incident bar. This modification is to increase the signal-to-noise ratio of weak transmitted signals. In a dynamic four-point bending experiment, force equilibrium between the two pairs of loading/supporting points may become an issue due to inertia and wave-propagation effects. If a specimen is loaded with a traditional trapezoidal-like Hopkinson bar incident pulse, sample vibration/resonance is expected because of the high-frequency components in the incident pulse, which imposes difficulties in interpreting the collected force signals. In this case, numeri-

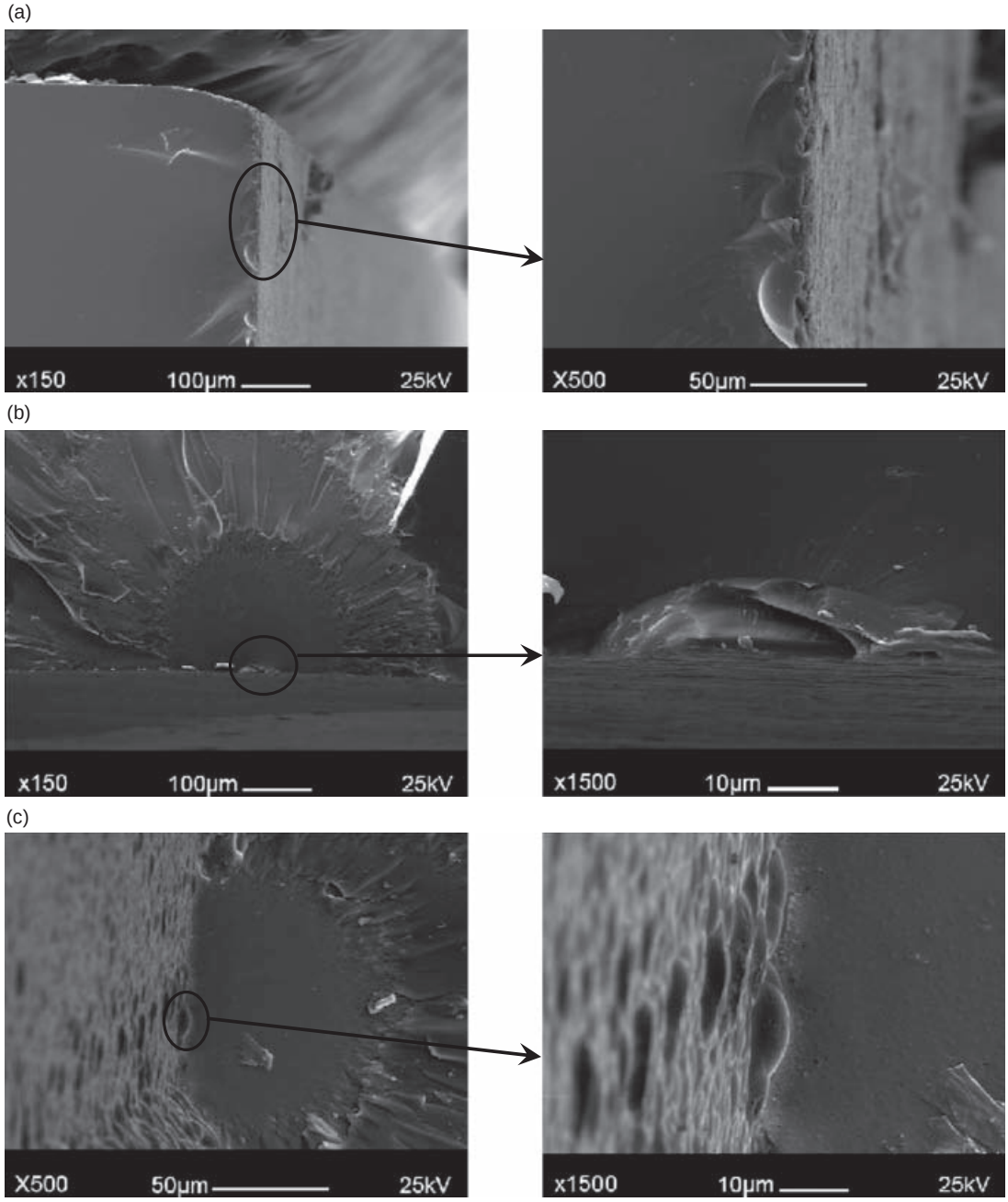

Fig. 9. Fracture surface and failure origins of different groups of glass samples. Flaw size is measured in terms of length and depth: (a) ground by 220-grit sandpapers (approximate flaw size 125 μm × 29 μm); (b) ground by 1500-grit sandpapers (approximate flaw size 57 μm × 11 μm); (c) polished and etched by HF acid (approximate flaw size 12 μm × 4 μm).

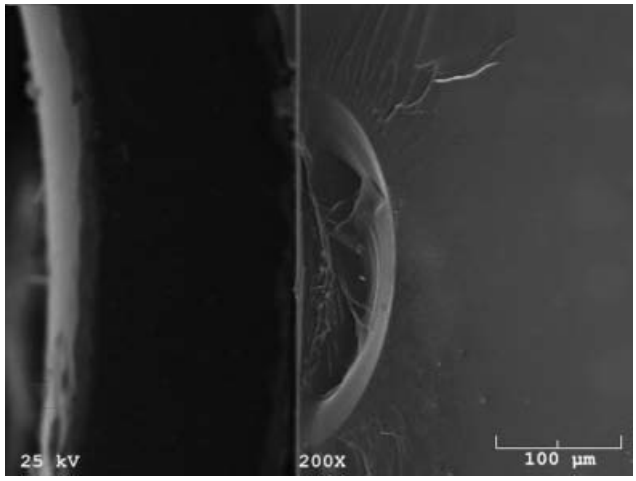

Fig. 10. Semielliptical subsurface mircocrack induced by Knoop indentation.

cal methods are often required in sample stress analysis. It is certainly desired that in strength-characterization experiments at high rates, inertia effects are minimized. In this study, we successfully avoided the potential vibration/resonance through control of the incident pulse shape. This is achieved by extending the rise time of the incident (loading) pulse from around 10 to ~160 μs, with a smooth transition to a plateau. This loading profile eliminates most of the high-frequency components in a conventional SHPB incident pulse and thus significantly reduces the possibility of exciting resonance in the beam specimen or causing wave dispersion along the bars. The plateau followed by the initial ramp is necessary for creating a constant loading rate at the tensile surface. Figure 6 shows the force equilibrium between the incident and transmitted load spans. Force vibration in the incident bar side was limited to the very beginning of the loading process. The nearly overlapping force histories recorded at the loading points and supporting points indicate that the specimen was subjected to an equilibrated loading history. Inertia effects were minimized. Figure 7 shows the time history of the loading rate. This is obtained by differentiating the stress–time profile in the transmission bar, which is also shown. It is seen that after increasing initially, the loading rate was maintained to around a constant value, which is important when the strength results need to be reported as a function of loading rates.

In a four-point bending experiment on a beam with a rectangular cross section, the maximum surface tensile stress is calculated as

$$\sigma(t) = \frac{3P(t)(L-l)}{2bd^2} \tag{1}$$

where l is the load span (incident bar side), L is the support span (transmission bar side), and b and d are the specimen width and height, respectively. $P(t)$ is the measured force history and the flexure strength is calculated using the maximum achieved value of P. In the experiments performed on the servohydraulic MTS machine, this force history is recorded by a load cell, while in SHPB experiments the force history in the specimen is calculated by

$$P(t) = EA\varepsilon_T(t) \tag{2}$$

where E and A are the Young's modulus and the cross-sectional area of the transmission bar, respectively; ε_T is the strain signal measured on the transmission bar. When the specimen fractures, the force history reaches its peak. The flexural strength is then calculated from this peak load using Eq. (1).

The variation in flexural strength as a function of the loading rate for all surface conditions is shown in Fig. 8. It is clear that the flexural strength of borosilicate glass increases with increasing loading rates in the loading-rate range achieved in this study, regardless of the surface conditions. Below the rate of 2500

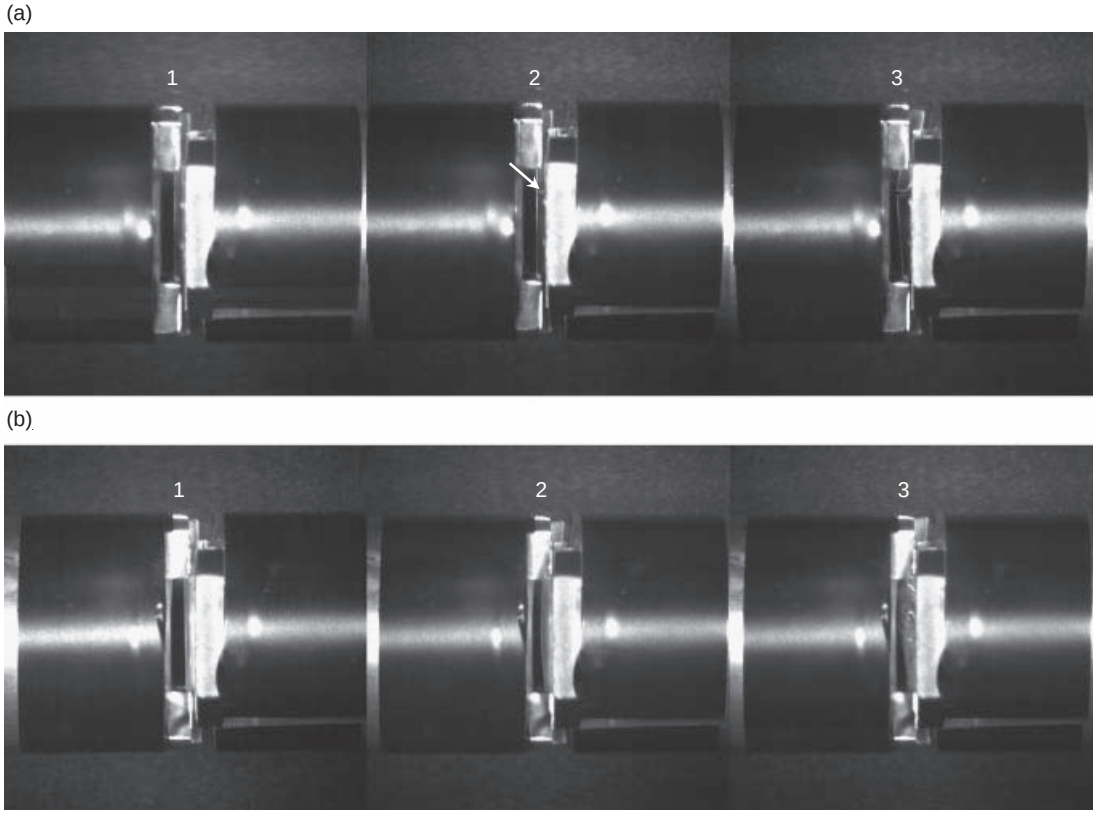

Fig. 11. High-speed camera images showing the typical dynamic failure of (a) sample ground by sandpapers; (b) sample etched by HF acid. White arrow indicates the through crack.

MPa/s, the flexural strength is roughly a linear function of the logarithm loading rate, whereas not much rate sensitivity is observed above 2500 MPa/s. For the group #1 and #2 samples, the particle size difference in sandpapers imposes only relatively small variations in the flexural strength. The average strength of group #2 samples is 60%–90% (depending on the loading rates) higher than that of group #1 samples. This strength improvement is achieved by an approximately 80% reduction in surface roughness. For group #3 samples, which were etched by HF acid, the average flexural strength is 700%–1500% higher than that of group #1 samples over the same loading-rate range. The average flexural strength of etched samples achieved at the highest loading rate is 1.1 GPa. The surface roughness values of the etched samples are actually higher than those of fine-ground samples (group #2). This observation indicates that the surface roughness value alone is not sufficient to relate the flexural strength to the surface quality of glass materials. SEM images on fracture surfaces and therefore examined to further investigate the failure mechanism of different groups of specimens. Failure origins in sandpaper-ground glass samples are observed to locate at the subsurface microcrack front, as is evident in Figs. 9(a) and (b), which are most likely being induced by indentation of abrasive particles. Such semielliptical microcracks are very similar in shape to those resulting from Knoop indentation, as shown in Fig. 10. Hence, the flexural strength of sandpaper-ground samples is governed by the sharp subsurface flaws. The observed differences in strength under different grinding conditions could also be explained by the differences in the flaw size. Figure 9(c) shows the fracture surface of an HF acid-etched sample. In this particular case, failure is initiated from right underneath a deep surface pit (not a sharp crack front). The acid-etching-induced surface flaw is much smaller in size compared with those semielliptical cracks, and no subsurface cracks are visible. These surface pits are blunt in nature so that the stress intensity is much less than that around a sharp subsurface crack front, which results in the high strength of etched samples.

A further look at the loading rate dependence on flexural strength reveals that for sandpaper-ground samples, the flexural strength increased by about 90% when the loading rate varied from 0.7×10^6 to 4×10^6 MPa/s, whereas for HF acid-etched samples, thus strength increase is about 200%. Because the only differences between those two groups of samples are the critical flaw types, the difference in the rate dependence of strength is considered to be the difference in the shapes of defects. Under a sharp indentation pit, cracks are formed and connected to the pit before global mechanical loading. On the other hand, under a pit blunted by HF acid, new cracks will have to form under the loading. A higher loading rate will cause multiple cracks to form simultaneously, which may account for the difference in the rate dependency.

To monitor the dynamic deformation and failure processes in the glass specimen, a high-speed digital camera along with a pair of strobe lights was synchronized with the SHPB to record the dynamic bending deformation and failure at high loading rates. The camera trigger was carefully set such that the entire deformation and fracture processes could be visualized. Thirty-two frames were taken in each experiment at a frame rate of 50 000 fps. The fracture of group #1 and #2 samples was found to be very similar, for which a typical image is shown in Fig. 11(a). A dominant crack was initiated from the tension side and propagated to the compression side, leading to the fracture of the beam specimen. However, when the tensile surface of the beam sample is polished and etched (group #3), the failure process is quite different, as shown in Fig. 11(b). While the specimen was intensively bent, multiple cracks were initiated and propagated through the sample. This occurred in an "explosive" manner and disassembled the sample into many tiny pieces. The dynamic compressive strength of this borosilicate glass is around 1.5 GPa, which was measured in a previous research.[1]

The tested samples were collected and the fracture surfaces were examined under an optical microscope. A set of fracture surface images taken on a specimen after the experiment at a 4×10^6 MPa/s loading rate are shown in Fig. 12. The sample cross section is 2 mm × 3 mm. For samples ground by a 220-grit sandpaper, fracture was initiated from surface-located strength-limiting flaws. The flaw is likely associated with a relatively large and deep machining groove or pit. For HF acid-etched samples and samples ground by a 1500-grit sandpaper, fracture is more likely to initiate from an edge-located, strength-limiting flaw. Similar results at a lower loading rate are also shown in Fig. 13. The stress concentrations on the edge flaws become more dominant as the surface tensile strength increases. Previous studies on the bending strength of borosilicate glass[33] showed that the edge defects should account for the low-strength behavior of unchamfered samples. However, in our current study, the failure of glass samples in four-point bending tests is actually a competing process between the surface flaws, which were intentionally introduced during various surface modifications, and

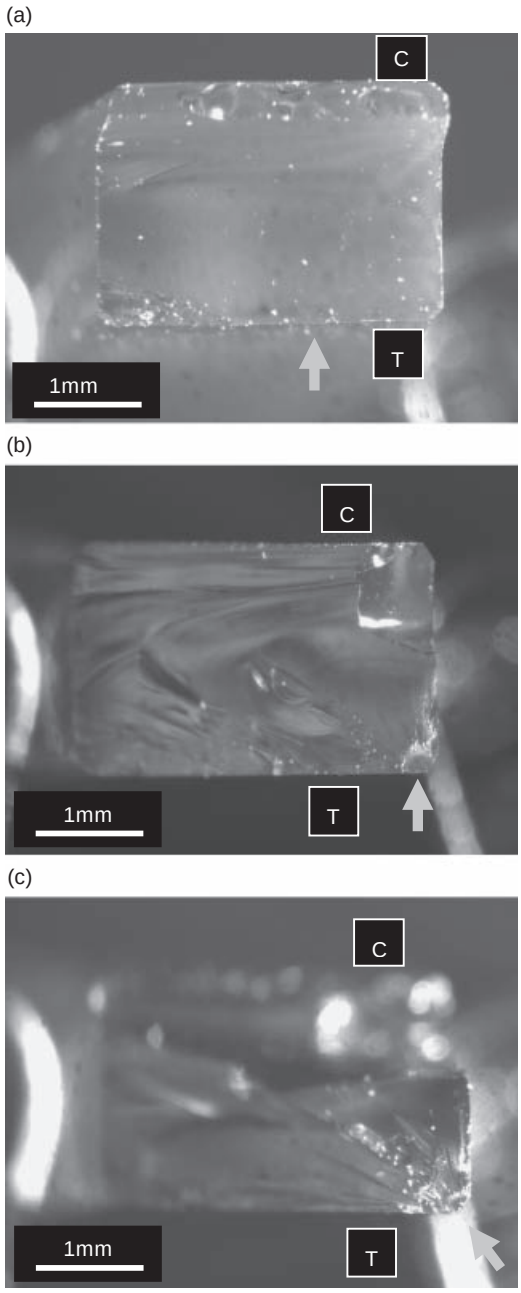

Fig. 12. Fracture surface morphology of samples tested at 4×10^6 MPa/s. (a) Sample ground by 220-grit sandpaper; (b) sample ground by 1500-grit sandpaper; (c) sample polished and then etched by HF acid. "C" and "T" represent "compression side" and "tension side," respectively. Arrows indicate crack initiation sites.

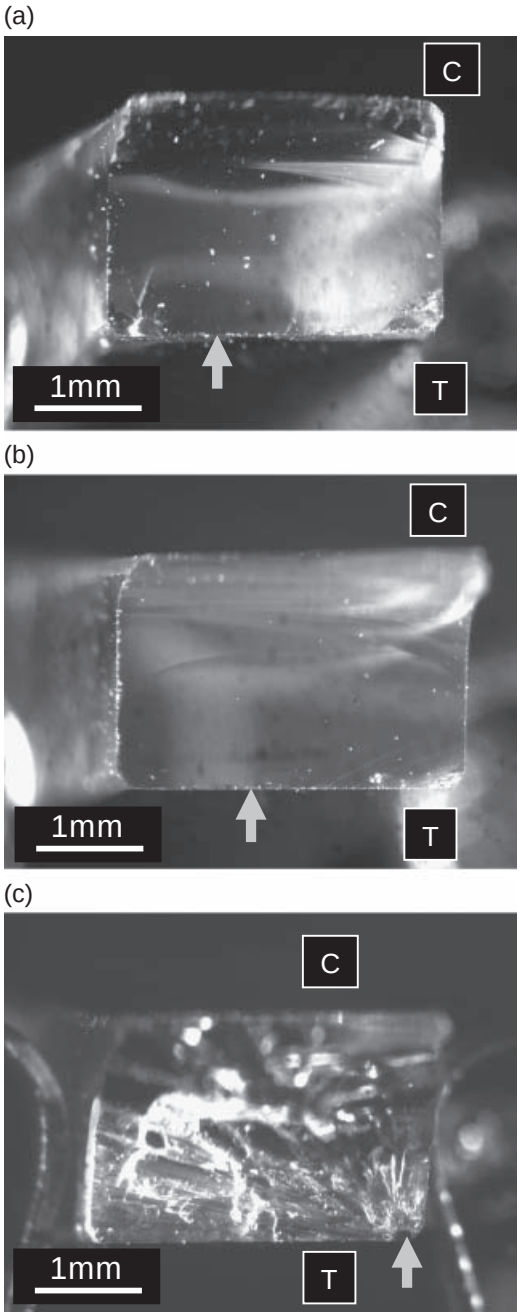

Fig. 13. Fracture surface morphology of samples tested at 0.7 MPa/s. (a) Sample ground by 220-grit sandpaper; (b) sample ground by 1500-grit sandpaper; (c) sample polished and then etched by HF acid. "C" and "T" represent "compression side" and "tension side," respectively. Arrows indicate crack initiation sites.

the edge flaws from chamfering. Chamfering on the edge both reduces the flaw size introduced by machining and removes the highly stress-concentrated corners. While the corners are removed, new flaws created by the chamfering procedure are located in less stress-concentrated areas. When the surface flaws became less severe, the glass failure underwent a transition from a surface flaw-dominated mode to an edge flaw-dominated mode. The chamfering procedure increased the stress level for this transition. On comparing Figs. 12 and 13, it is evident that the surface quality level required for this transition increased with decreasing loading rate. This could be attributed to the fact that the ultimate tensile strength at a lower rate decreases drastically for all the surface conditions investigated, and thus a higher surface quality level is required to satisfy the transition stress. Because of the premature failure from the edge flaws, the intrinsic tensile strength of the etched samples is expected to be higher than the currently measured values. The failure initiation sites have raised challenges in the accurate characterization of the flexural strength of borosilicate glass under desired surface conditions. Further expansion of the current experimental technique is desired in order to eliminate edge flaws.

IV. Summary

Quasistatic and dynamic flexural experiments were conducted on a borosilicate glass under different surface conditions. The dynamic experiments were carried out on a modified SHPB setup. A pulse-shaping technique was used to subject the specimen to constant loading rates. The surface conditions of the tensile surfaces of the samples were varied to study their effects on the flexural strength of the glass. A sample flexural strength of 1.1 GPa at high loading rates was measured on specimens where the tensile surfaces were chemically etched. The flexural strength of the borosilicate glass increases with increasing loading rate for all the surface conditions studied. For the ground samples, the flexural strength decreases with increasing surface roughness, while the etched samples possess high strength although at high surface roughness. SEM image analysis of the fracture surfaces shows that small, blunt surface pits are the failure initiation sites for acid-etched samples, while large, sharp sub-surface cracks are identified as fracture origins for the sandpaper-ground samples.

High-speed camera images reveal that a dominating crack from a tensile surface flaw governs the fracture initiation in most ground samples. Multiple crack initiation was observed in the failure of the samples with etched tensile surfaces. Optical microscopy images showed that flaws caused from chamfering and located at specimen edges are the crack initiation sites for specimens possessing high flexural strengths. This fact suggests the need to extend the current four-point bending experiment to equibiaxial flexural experiments to circumvent the effects of edges on flexural strength.

References

[1]X. Nie, W. Chen, X. Sun, and D. Templeton, "Dynamic Failure of Borosilicate Glass Under Compression/Shear Loading," *J. Am. Ceram. Soc.*, **90** [8] 2556–62 (2007).

[2]K. A. Dannemann, A. E. Nicholls, C. E. Anderson Jr., I. S. Chocron, and J. D. Walker, "Compression testing and response of borosilicate glass: intact and damaged"; *Proceedings of Advanced Ceramics and Composites Conference*, Cocoa Beach, FL, January 23–27, 2006.

[3]A. S. Vlasov, E. L. Zilberbrand, A. A. Kozhushko, A. I. Kozachuk, and A. B. Sinani, "Behavior of Strengthened Glass Under High-Velocity Impact," *Strength Mater.*, **34** [3] 266–8 (2002).

[4]M. Hara, "Some Aspects of Strength Characteristics of Glass," *Glastech. Ber.*, **61**, 191–6 (1988).

[5]B. P. Bandyopadhyay, "The Effects of Grinding Parameters on the Strength and Surface Finish of Two Silicon Nitride Ceramics," *J. Mater. Process. Technol.*, **53**, 533–43 (1995).

[6]D. M. Liu, C. T. Fu, and L. J. Lin, "Influence of Machining on the Strength of SiC–Al_2O_3–Y_2O_3 Ceramic," *Ceram. Int.*, **22**, 267–70 (1996).

[7]M. Guazzato, M. Albakry, L. Quach, and M. V. Swain, "Influence of Grinding, Sandblasting, Polishing and Heat Treatment on the Flexural Strength of a Glass-Infiltrated Alumina-Reinforced Dental Ceramic," *Biomaterials*, **25**, 2153–60 (2004).

[8]J. E. Ritter Jr. and C. L. Sherburne, "Dynamic and Static Fatigue of Silicate Glasses," *J. Am. Ceram. Soc.*, **54** [12] 601–5 (1971).

[9]J. E. Ritter and M. R. Lin, "Effect of Polymer Coatings on the Strength and Fatigue Behavior of Indented Soda-Lime Glass," *Glass Technol.*, **32** [2] 51–4 (1991).

[10]J. J. Mecholsky Jr., S. W. Freiman, and R. W. Rice, "Effect of Grinding on Flaw Geometry and Fracture of Glass," *J. Am. Ceram. Soc.*, **60** [3–4] 114–7.

[11]G. Scott Glaesemann, K. Jakus, and J. E. Ritter Jr., "Strength Variability of Indented Soda-Lime Glass," *J. Am. Ceram. Soc.*, **70** [6] 441–4 (1987).

[12]C. Gurney, "Source of Weakness in Glass," *Proc. R. Soc. Lond.*, **282** [1388] 24–33 (1964).

[13]I. W. Donald, "Methods for Improving the Mechanical Properties of Oxide Glasses," *J. Mater. Sci.*, **24**, 4177–208 (1989).

[14]C. Symmers, J. B. Ward, and B. Sugarman, "Studies of the Mechanical Strength of Glass," *Phys. Chem. Glasses*, **3**, 76–83 (1962).

[15]C. K. Saha and A. R. Cooper, "Effect of Etched Depth on Glass Strength," *J. Am. Ceram. Soc.*, **67** [8] C158–60 (1984).

[16]G. T. Gray, "Classic Split Hopkinson Pressure Bar Technique"; pp. 462–76, in *ASM Handbook, Vol. 8, Mechanical Testing and Evaluation*. Edited by H. Kuhn and D. Medlin. ASM International, Materials Park, OH, 2000.

[17]H. Kolsky, "An Investigation of the Mechanical Properties of Materials at Very High Rates of Loading," *Proc. R. Soc. Lond.*, **B62**, 676–700 (1949).
[18]B. Paliwalw, K. T. Ramesh, and J. W. McCauley, "Direct Observation of the Dynamic Compressive Failure of a Transparent Polycrystalline Ceramic (AlON)," *J. Am. Ceram. Soc.*, **89** [7] 2128–33 (2006).
[19]B. Song and W. Chen, "Split Hopkinson Bar Techniques for Characterizing Soft Materials," *Lat. Am. J. Solids Struct.*, **2**, 113–52 (2005).
[20]B. Song, Y. Ge, W. Chen, and T. Weerasooriya, "Radial Inertia Effects in Kolsky Bar Testing of Extra-Soft Specimens," *Exp. Mech.*, **47**, 659–70 (2007).
[21]T. Weerasooriya, P. Moy, D. Casem, M. Cheng, and W. Chen, "A Four-Point Bend Technique to Determine Dynamic Fracture Toughness of Ceramics," *J. Am. Ceram. Soc.*, **89** [3] 990–5 (2006).
[22]ASTM C 1421-01b. "Standard Test Methods for Determination of Fracture Toughness of Advanced Ceramics at Ambient Temperatures"; in *Annual Book of ASTM Standards*. ASTM, West Conshohocken, PA, 2001.
[23]ASTM C 1161-02c. "Standard Test Method for Flexural Strength of Advanced Ceramics at Ambient Temperature," *Annual Book of ASTM Standards*. ASTM, West Conshohocken, PA, 2003.
[24]C. A. Ross, D. M. Jerome, J. W. Tedesco, and M. L. Hughes, "Moisture and Strain Rate Effects on Concrete Strength," *ACI Mater. J.*, **93**, 293–300 (1996).
[25]W. Chen and G. Ravichandran, "Dynamic Compressive Behavior of a Glass Ceramic Under Lateral Confinement," *J. Mech. Phys. Solids*, **45** [8] 1303–28 (1997).
[26]S. Sarva and S. Nemat-Nasser, "Dynamic Compression Strength of Silicon Carbide Under Uniaxial Compression," *Mater. Sci. Eng. A*, **A317**, 140–4 (2001).
[27]M. Cheng, W. Chen, and K. R. Sridhar, "Experimental Method for a Dynamic Biaxial Flexural Strength Test of Thin Ceramic Substrates," *J. Am. Ceram. Soc.*, **85** [5] 1203–9 (2002).
[28]Y. Zheng, J. M. Vieira, F. J. Oliveira, J. P. Davim, and P. Brogueira, "Relationship Between Flexural Strength and Surface Roughness for Hot-Pressed Si_3N_4 Self-Reinforced Ceramics," *J. Eur. Ceram. Soc.*, **20**, 1345–53 (2000).
[29]G. Bhamra, W. M. Palin, and G. J. P. Fleming, "The Effect of Surface Roughness on the Flexure Strength of an Alumina Reinforced All-Ceramic Crown Material," *J. Dent.*, **30**, 153–60 (2002).
[30]E. Le Bourhis, *Glass*, pp. 78–81. Wiley-VCH, Weinheim, 2008.
[31]B. A. Proctor, "Fracture of Glass," *Appl. Mater. Res.*, **3**, 28–34 (1964).
[32]V. M. Sglavo, R. Dal Maschio, and G. D. Soraru, "Effect of Etch Depth on Strength of Soda-Lime Glass Rods by a Statistical Approach," *J. Eur. Ceram. Soc.*, **11**, 341–6 (1993).
[33]M. H. Dielhof, L. J. M. G. Dortmans, and G. de With, "Fractography of Borosilicate Glass Tested in Three- and Four-Point Bending," *J. Eur. Ceram. Soc.*, **12**, 215–20 (1993). □